Available online at www.sciencedirect.com
ScienceDirect
International Journal of Solids and Structures 45 (2008) 1406–1429
INTERNATIONAL JOURNAL OF SOLIDS AND STRUCTURES
www.elsevier.com/locate/ijsolstr

A micromechanical model of elastoplastic and damage behavior of a cohesive geomaterial

A. Abou-Chakra Guéry [a,b,*], F. Cormery [b], J.F. Shao [b], D. Kondo [b]

[a] *Agence Nationale pour la gestion des déchets radioactifs (ANDRA), 92296 Chatenay Malabry, France*
[b] *Laboratory of Mechanics of Lille, UMR 8107, Cité scientifique, 59655 Villeneuve d'Ascq, France*

Received 22 February 2007; received in revised form 23 August 2007
Available online 4 October 2007

Abstract

The present study is devoted to the development and validation of a nonlinear homogenization approach of the mechanical behavior of Callovo-Oxfordian argillites. The material is modeled as an heterogeneous composite composed of an elastoplastic clay matrix and of linear elastic or elastic damage inclusions. The macroscopic constitutive law is obtained by adapting the incremental method proposed by Hill [Hill, R., 1965. Continuum micro-mechanics of elastoplastic polycrystals. J. Mech. Phys. Solids 13, 89–101]. The approach consists in formulating the macroscopic tangent operator of the material by considering the nonlinear local behavior of each phase. Due to the matrix/inclusion morphology of the microstructure of the argillite, a Mori–Tanaka scheme is considered for the localization step. The developed model is first compared to Finite Element calculations and then validated and applied for the prediction of the macroscopic stress–strain responses of argillites.

Keywords: Geomaterials; Nonlinear homogenization; Plasticity and damage; Dilatancy; Unilateral effects; Experimental validation; Rocks micromechanics

1. Introduction

This study is performed in the general context of the project of underground disposal of radioactive waste, undertaken by the French National Radioactive Waste Management Agency (ANDRA). Its objective is to formulate a predictive constitutive model of the Callovo-Oxfordian argillite, a geological material chosen as one of possible geological barriers to radionuclides. Various phenomenological models have been proposed in the past for this class of materials. For instance Chiarelli et al. (2003) and Conil et al. (2004) developed a phenomenological modeling approach which couples plasticity and damage. The plastic behavior is of non-associated type with a particular emphasis on the plastic dilatancy (positive volumetric strains) while the

* Corresponding author. Address: Agence Nationale pour la gestion des déchets radioactifs (ANDRA), 92296 Chatenay Malabry, France. Tel.: +33 03 20 43 45 50; fax: +33 03 20 33 71 53.
E-mail address: ariane.guery@polytech-lille.fr (A. Abou-Chakra Guéry).

0020-7683/$ - see front matter © 2007 Elsevier Ltd. All rights reserved.
doi:10.1016/j.ijsolstr.2007.09.025

damage component of the model allows to describe the deterioration of the material properties. This model has been calibrated by making use of data from experiments on the Callovo-Oxfordian argillites and provides good predictions in terms of macroscopic stress–strain relations corresponding to various monotonic and cyclic compressive loading paths. Despite these predictions, these models are not able to take into account deformation mechanisms related to material heterogeneities.

Therefore, it is useful to develop a more physical modeling approach for this class of materials. The methodology followed in the present study consists to develop a constitutive model of hard clays by making use of a nonlinear homogenization approach. Various nonlinear homogenization techniques have been developed in the literature. Mention can be made of the so-called secant formulations by Berveiller and Zaoui (1979); Ponte-Castañeda and Suquet (1998); and Tandon and Weng (1988) for which the nonlinear local behavior of each phase is described by considering a secant stiffness corresponding to an appropriate effective deformation. More recently, Ponte-Castañeda (1991) and Willis (1989) proposed variational methods which deliver bounds for the nonlinear macroscopic behavior. However, it must be emphasized that the secant moduli techniques as well as the variational approach apply only to nonlinear constitutive behaviors deriving from a single potential, such as nonlinear elasticity or viscoplasticity when elastic effects are neglected. They are also generally limited to monotonous and radial loading paths.

Owing to the complexity of loading paths which are involved in the project of underground storage of radioactive waste, we have to adopt an incremental formulation instead of the above mentioned methods. For this purpose, we consider the Hill incremental method (Hill, 1965) which consists, at each loading step, in determining the macroscopic tangent moduli from the local tangent behavior of the different constituents. The incremental approach has been recently considered by various authors for two phase composites; for instance Chaboche and Kanouté (2005) applied and discussed this method to metals plasticity with classical J_2 theory whereas Doghri and Ouaar (2003) considered also a cyclic plasticity with a nonlinear kinematic hardening. In these studies, a brief account of the interest of the incremental method is done in comparison with other methods such as the tangent approaches proposed by Molinari et al. (1987) and Masson et al. (2000). In particular, by a combination of the basic Hill's approach with an "isotropization procedure", it was demonstrated that the method leads to efficient predictions.

The objective of the present study is mainly to implement the incremental method for the modeling of a three phase material, namely the argillite which is constituted of a plastic clay matrix and elastic or damaged mineral inclusions. In addition to the coupling between plasticity and damage, the originalities of the study lie in the consideration of non-associated and dilatant plasticity for the clay matrix and the extensive validation of the homogenized constitutive law by comparison with experimental data on different loading paths.

The outline of the paper is as follows. In Section 2, we describe the microstructure of the studied material and present the salient features of its macroscopic mechanical behavior under compressive loadings. Then, the principle and the formulation of the incremental method in the case of a three phase medium are recalled for its application to the argillite material (see Section 3). Section 4 is devoted to the formulation of the local behavior of the different constituents. In particular, a rigorous formulation is proposed in order to include unilateral effects (due to microcracks closure) in the damage modeling. These local constitutive laws are implemented in the nonlinear homogenization procedure in order to derive the homogenized law which is first validated by comparison with unit cell (Finite Element) calculations. In the last section, the proposed model is calibrated and experimentally validated for the Callovo-Oxfordian argillite.

2. Experimental observations on the Callovo-Oxfordian argillite behavior

2.1. Microstructure and mineralogical composition of the material

The material studied here is a sedimentary rock called Callovo-Oxfordian argillite, from the site where the underground research laboratory for nuclear waste disposal is operated by ANDRA. The Callovo-Oxfordian argillite layer is about 130 m thick referred by ANDRA as C2. Five lithostratigraphic units are characterized by different facies and mineralogical composition, subscripted C2a, C2b1, C2b2, C2c, and C2d, from base to top. Only three units of Oxfordian age (C2b1, C2b2, and C2c) are dealt with here and named depth 1, 2, and 3.

Experimental tests have been conducted on samples cored from the borehole EST 104 and from depth 1 between 451.4 to 466.8 m, depth 2 between 468.9 to 469.1 m, and depth 3 between 482.1 to 482.4 m.

Mineralogical compositions, initial porosity, and natural water content of samples were first investigated. Mineralogy was obtained from results of X-ray diffractometry and calcimetry that showed a composition of quartz (23% average), calcite (28% average), and clay minerals (45% average) together with subordinate feldspars, pyrite, and iron oxides (5% average). The clay minerals composition is relatively constant at 65% I/S (illite–smectite interstratified minerals), 30–35% illite, and 0–5% kaolinite and chlorite. We can notice a variation in mineralogical composition with depth as we can see in Fig. 1.

At the microscopic level, quartz and large calcite grains are scattered in a fine matrix of clay minerals and calcite which acts to cement the larger grains (see Fig. 2). Mineral grains have principally a rounded shape and a dimension between 10 and 40 μm. The clay minerals are grouped in clusters of some microns large that can coat very well the grain form.

From microstructural observations, Gasc (1999) has observed the presence of clay particles in the layer of sheets, including quartz and calcite crystal grains. She noted that the carbonated phase does not constitute a cement but is organized in grains spread in a clay matrix. Chiarelli et al. (2003) remark in the same way that quartz and calcite grains are tied to the clay matrix. In Fig. 2, we observe that calcite and quartz particles are dispersed in the clayed matrix.

The first stage of the homogenization procedure is the definition of the representative volume element (r.v.e.). The previous analyses lead us to consider the argillite as a three phase composite of inclusion/matrix type in which we discern the calcite and quartz phases supposed spherical and distributed isolately in a clay matrix.

Other microstructural observations bring to light a lot of clay minerals extruded. This could be due to a relative slide movement between the slices provoking the manifestation of residual plastic deformations observed during macroscopic tests in the axial and lateral directions after unloading.

Relying on microscopic analysis, it can be remarked as well that mechanical properties of the argillite minerals are very contrasted (the Young modulus for quartz and calcite is about 100 GPa whereas the clay matrix

Depth(m)	Calcite content (%)	Quartz content (%)	Clays content (%)
Depth 1 : 451.4-466.8	20-40	20-30	40-55
Depth 2 : 468.9-469.1	25-55	20-30	35-55
Depth 3 : 482.1-482.4	25-35	15-20	45-60

Fig. 1. Mineral compositions and basic properties of Callovo-Oxfordian argillite.

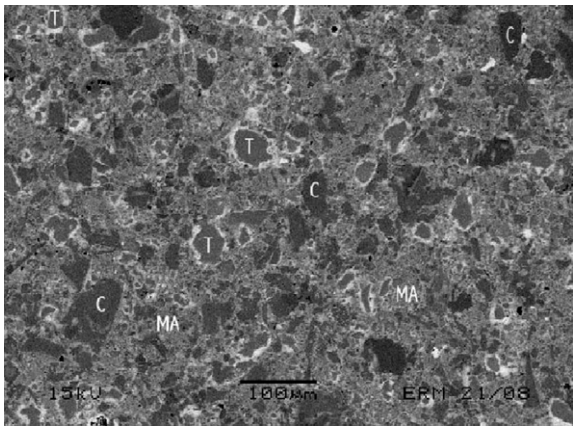

Fig. 2. Micrography of a typical Callovo-Oxfordian argillite structure: calcite grains (C), quartz grains (tectosilicates) (T), and clay matrix (MA).

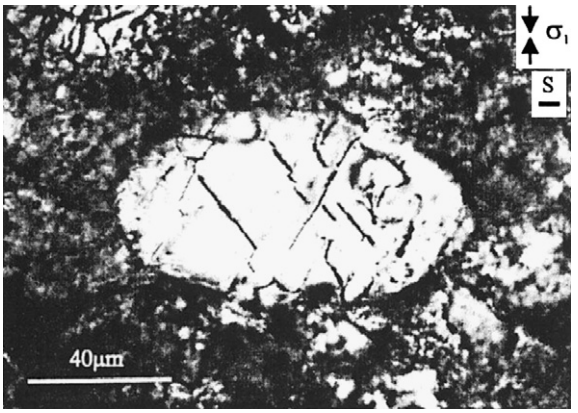

Fig. 3. Micrography of a calcite grain with transgranular fractures.

has a modulus which value is about 10 GPa). In that manner, it can lead to high local deformations in the clay matrix regarding to those in the calcite and quartz grains. This contrast leads to shearing stress concentration in the interfaces and can generate microcracks by decohesion at the grains/matrix boundaries or transgranular fractures. The cracking inside the grains are mainly visible in the calcite (Fig. 3) in which a network of microcracks randomly oriented and quite uniformly distributed can be observed. For the sake of simplicity, we assume an isotropic damage in this work. We will neglect as well the microcracking by decohesion to suppose that the only constituent who has an elastic damaged behavior is the calcite. This damage induced by microcracks can explain the degradation of the stiffness in the lateral direction observed during argillite macroscopic tests.

Therefore, we will suppose after that an isotropic, linear, and elastic behavior for the quartz grains, a damaged elastic behavior for the calcite grains with microcracks randomly distributed and an elastoplastic behavior for the clay matrix.

2.2. Brief summary of the macroscopic behavior of the material

Basic macroscopic behavior of argillite is here briefly recalled in order to show the coherence with microscopic analyses. Hydrostatic and triaxial compression tests have been performed by Chiarelli et al. (2003). The range of confining pressure is from 0 to 20 MPa, which was chosen according to the estimation of in situ stresses. Unloading–reloading cycles of deviatoric stress were included in each test in order to evaluate the progressive deterioration of elastic stiffness and the macroscopic plastic deformation. The experimental results from hydrostatic compression tests have shown that there is a small difference of strain between the directions parallel and perpendicular to the natural bedding plane (see Chiarelli et al., 2003). This indicates an initial anisotropy of the Callovo-Oxfordian argillite, which seems to be quite small and can be neglected. Triaxial compression tests have been performed by axial strain controlled path with an average rate of $\dot{\varepsilon} = 6 \times 10^{-6}/\mathrm{s}$. This will justify the quasi static analysis of the material behavior considered in the present study. It is important to precise here the convention used for the stress–strain diagram.

For a triaxial compression test the matrix of the components of the stress tensor reads in the cartesian basis:

$$[\boldsymbol{\Sigma}] = \begin{pmatrix} \Sigma_{11} & 0 & 0 \\ 0 & \Sigma_{33} & 0 \\ 0 & 0 & \Sigma_{33} \end{pmatrix} \tag{1}$$

where Σ_{11} represents the axial stress and Σ_{33} the lateral stress. The convention adopted is that Σ_{11} and Σ_{33} are positive for tension test and negative for compression test. Typical stress–strain curves from triaxial compression tests have shown two basic phenomena on the macroscopic mechanical responses of the argillite (Fig. 5).

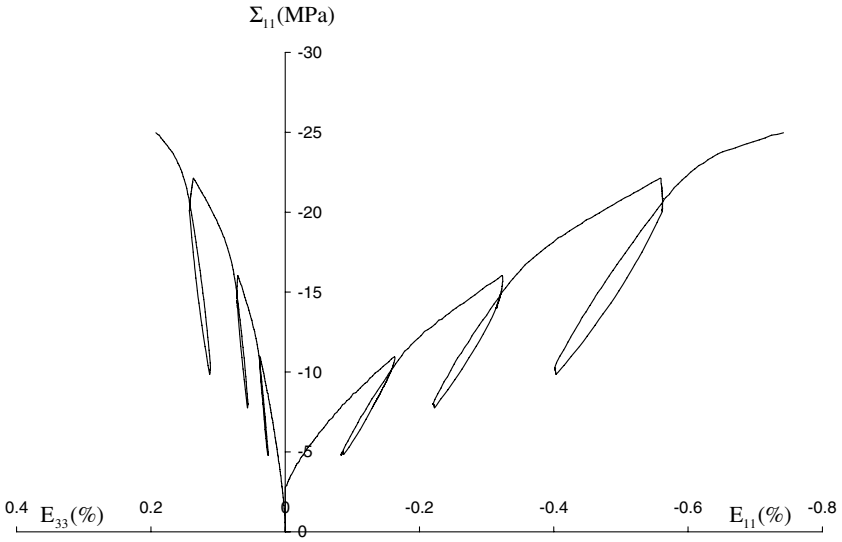

Fig. 4. Example of stress–strain curves from an uniaxial compression test with unloading–reloading cycles. Depth 3, with $f_0 = 60\%$, $f_1 = 26\%$, and $f_2 = 14\%$.

First, large residual strains are observed both in the axial (E_{11}) and lateral (E_{33}) directions after unloading of deviatoric stress. This is observed in all the tests including uniaxial compression (Fig. 4).

In connection with the microscopic analysis mentioned above, such irreversible strains are essentially related to plastic deformation by clay sheet sliding. Secondly, by determination of elastic stiffness during the unloading–reloading cycles, a progressive decrease of the elastic stiffness is obtained as a function of applied stress level. The degradation of the stiffness in the lateral direction is more important than in the axial one. Also, in connection with the analysis of microstructure of the argillite, this degradation of elastic properties can be considered as a consequence of induced damage by microcracks in calcite phase.

Further, influences of mineralogical composition on mechanical behavior of argillite have also been studied. The macroscopic elastic modulus increases with calcite content while it decreases with clay content. The Poisson's ratio is nearly insensitive to all the mineralogical constituents. Mineralogical compositions strongly affect both plastic deformation and induced damage. Roughly, at the same stress level, it is found that plastic strains decrease when calcite content increases, but become more important when quartz or clay content increases. The induced damage increases with calcite content.

3. Incremental formulation of the homogenized constitutive law

The objective of this section is to formulate the macroscopic constitutive law of the Callovo-Oxfordian argillite from a nonlinear homogenization approach, namely the Hill's incremental method (Hill, 1965). After recalling the basic principle of this nonlinear homogenization method, the computation of the tangent localization operator required for its implementation is detailed.

3.1. Principle of the method

As already stated, the Callovo-Oxfordian argillite can be represented by a three phases composite with distinct mechanical properties. This material has a matrix–inclusion morphology with phases randomly distributed, the calcite and quartz minerals being embedded in the clay matrix.

The first step in the homogenization process is the relevant choice of scales for the study of the mechanical behavior. The microscale (at which the dissipation mechanisms occur) is fixed by the heterogeneities size, about 10 μm. Considering phenomena at a smaller scale would lead to a model not easy to be implemented for a engineering analysis. Therefore, it is possible to define a representative volume element (r.v.e.) giving

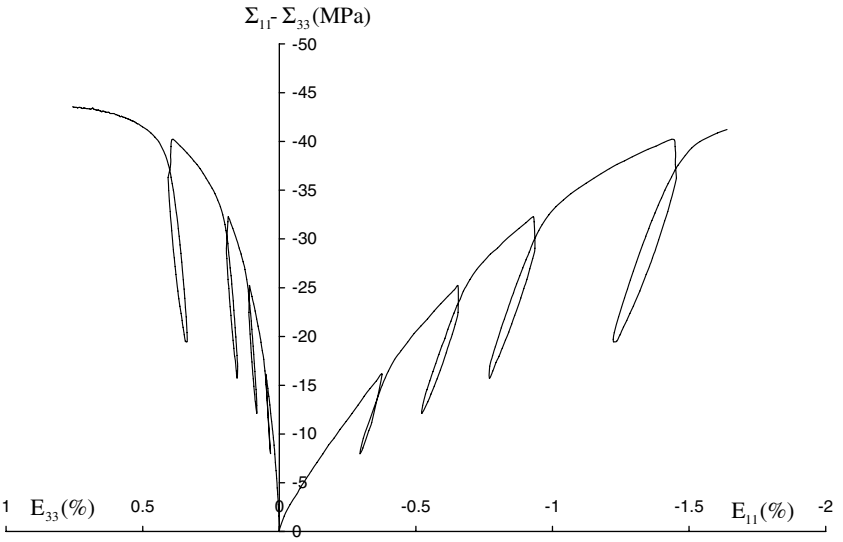

Fig. 5. Example of stress–strain curves from a triaxial compression test under 10 MPa confining pressure with unloading–reloading cycles. Depth 3, with $f_0 = 60\%$, $f_1 = 26\%$, and $f_2 = 14\%$.

the main statistical informations associated with the repartition and the morphology of the argillite heterogeneities. As classically, the conditions for the scale separation are assumed to be fulfilled. This is verified by the dimensions of the samples tested in the experimental part of the study. In the incremental homogenization method, adopted in the present study, the r.v.e, named V, is subjected to an uniform strain rate on the boundary (Fig. 6). V_r and f_r (where $r = 0, 2$) are the volume and the volume fraction of the phase r, respectively. The compact notations $\bar{l}$ and $\bar{l}_r$ will be used to denote the average of a field l in the entire r.v.e. V and that in each phase V_r, such as

$$\bar{l} = \langle l \rangle = \sum_{r=0}^{2} f_r \bar{l}_r, \quad \bar{l}_r = \langle l \rangle_r = \frac{1}{|V_r|} \int_{V_r} l(\underline{x}) \, \mathrm{d}\underline{x} \tag{2}$$

The methodology of the incremental method by Hill (1965) consists to derive the overall tangent operator from the knowledge of the local behaviors. It requires a rate formulation of the local behaviors of the constituents:

$$\dot{\underline{\underline{\sigma}}}(\underline{x}) = \mathbb{L}(\underline{x}) : \dot{\underline{\underline{\varepsilon}}}(\underline{x}) \tag{3}$$

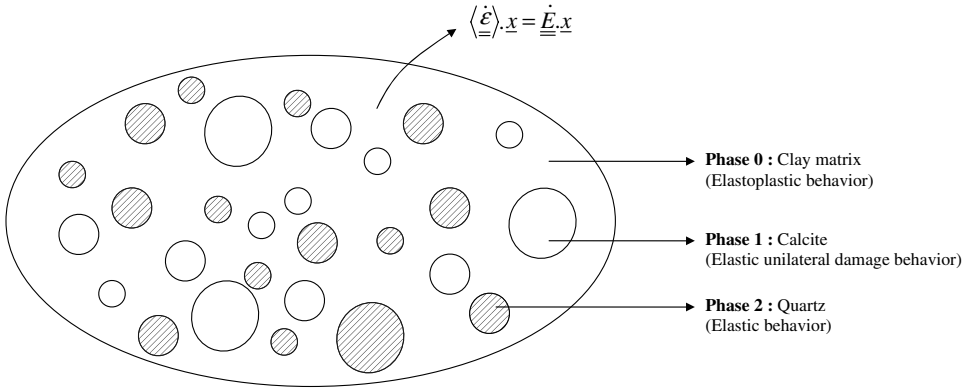

Fig. 6. Representative volume element (r.v.e) of the Callovo-Oxfordian argillite.

Since this local behavior takes the form of a linearized law with nonlinear tangent moduli, it follows that classical Eshelby-based homogenization procedures (Eshelby, 1957) can be used for the resolution of the problem. For this purpose, a tangent localization tensor $\mathbb{A}$ which relates the local strain rate to the macroscopic strain rate has to be introduced:

$$\dot{\underline{\underline{\varepsilon}}}(\underline{x}) = \mathbb{A}(\underline{x}) : \dot{\underline{\underline{E}}} \tag{4}$$

The macroscopic stress rate reads then:

$$\dot{\underline{\underline{\Sigma}}} = \mathbb{L}^{\text{hom}} : \dot{\underline{\underline{E}}} \tag{5}$$

where the macroscopic tangent operator $\mathbb{L}^{\text{hom}}$ is given by

$$\mathbb{L}^{\text{hom}} = \langle \mathbb{L} : \mathbb{A} \rangle \tag{6}$$

Further, the homogenization procedure should verify the energy condition of Hill, $\dot{\underline{\underline{\Sigma}}} : \dot{\underline{\underline{E}}} = \dot{\underline{\underline{\sigma}}} : \dot{\underline{\underline{\varepsilon}}}$.

3.2. Determination of the anisotropic tangent localization tensor

For the implementation of the incremental method, we need an approximation of the tangent operator in each phase:

Hypothesis. *At any point $\underline{x}$ of the phase (r),*[1] *the relation between the strain rate and the stress rate can be approximated by*

$$\forall \underline{x} \in (r), \quad \dot{\underline{\underline{\sigma}}}(\underline{x}) = \mathbb{L}_r : \dot{\underline{\underline{\varepsilon}}}(\underline{x}) \tag{7}$$

In practice, $\mathbb{L}_r$ is evaluated for a reference state $\underline{\underline{\varepsilon}}_r$ classically chosen as the average of the strain field in the phase (r). In this way to consider the problem it is assumed that each phase has an uniform moduli while in reality the strain field around and inside the inclusion is strongly heterogenous. The localization relation (4) reads then:

$$\dot{\underline{\underline{\varepsilon}}}_r = \mathbb{A}_r : \dot{\underline{\underline{E}}} \tag{8}$$

where $\mathbb{A}_r$ is the constant localization tensor, in the phase which is computed by using the Mori and Tanaka (1973) scheme originally devoted to two-phase materials. Furthermore, the calcite and quartz grains are assumed to be spherical inclusions. For multi-phase composite, we adopt a direct extension of the Mori–Tanaka scheme which may lead in some cases to non-physical results (cf. Benveniste, 1991) but is relevant here because spherical inclusions are considered. The localization tensor $\mathbb{A}_r$ associated with this scheme classically takes the form:

$$\begin{cases} \mathbb{A}_r = \mathbb{T}_r : \left[\sum_r f_r \mathbb{T}_r\right]^{-1} \\ \mathbb{T}_r = \left[\mathbb{I} + \mathbb{P}^0_{I_r} : (\delta\mathbb{L}_r)\right]^{-1} \\ \delta\mathbb{L}_r = \mathbb{L}_r - \mathbb{L}_0 \end{cases} \tag{9}$$

in which $\mathbb{P}^0_{I_r}$ is the so-called Hill tensor which depends on both the geometry of the inclusions r (considered here as spheres) and on the tangent operator $\mathbb{L}_0$ of the clay matrix.

Since for the dilute scheme (valid in the case of non-interacting inclusions), the localization tensor $\mathbb{A}_r$ coincides with $\mathbb{T}_r$ (see Eshelby, 1957), it is clear that the interaction between the different phases is taken into account in (9) by mean of the term $[\sum_r f_r \mathbb{T}_r]^{-1}$.

As the calcite and quartz grains have the same geometry, we will denote $\mathbb{P}^0_{I_1} = \mathbb{P}^0_{I_2} = \mathbb{P}^0_I$ with:

[1] (0) is the clay phase, (1) is the calcite phase, and (2) the quartz phase.

$$\mathbb{P}_I^0 = \mathbb{S}^E(\mathbb{L}_0) : \mathbb{L}_0^{-1} \tag{10}$$

Due to the anisotropy of the tangent operator $\mathbb{L}_0$, an analytical determination of the Hill tensor $\mathbb{P}_I^0$ is not possible in general. A numerical integration procedure is needed (cf. Ghahremani, 1977; Gavazzi and Lagoudas, 1990).

Reporting (9) into (6), the homogenized tangent operator is then written as follows:

$$\mathbb{L}^{\text{hom}} = \sum_r f_r \mathbb{L}_r : \mathbb{A}_r, \quad r = 0 \text{ to } 2 \tag{11}$$

where f_r is the concentration of the phase (r).

The application of the incremental method requires to determine the tangent operators of the different phases. The tangent moduli $\mathbb{L}_0$ associated with the plastic matrix and $\mathbb{L}_1$ with the damaged elastic phase will be determined in the next section (see relations (25) and (45), respectively). The tangent operator of the elastic phase is noted as $\mathbb{L}_2$ equal to the elastic stiffness of the constituent.

4. Modeling of the local constituents behaviors

Based on the microstructural observations and mechanical data, as underlined before (see Section 2.1), the clay matrix is modeled as an elastoplastic constituent while the quartz is considered as linear elastic and the behavior of calcite grains is described by means of an elastic damage model. For the calcite phase a particular attention is paid to the consideration of the unilateral effect due to damage.

4.1. Elastoplastic behavior of the clay phase

An elastoplastic behavior is assumed for the clay matrix. A non-associated plastic model based on a Drucker–Prager criterion with isotropic hardening is proposed (Drucker and Prager, 1952). As classically, the free energy associated with the elastoplastic behavior is the sum of the elastic strain energy and the locked energy due to plastic hardening $W^\gamma(\gamma^p)$:

$$W(\underline{\underline{\varepsilon}}, \beta) = \tfrac{1}{2}(\underline{\underline{\varepsilon}} - \underline{\underline{\varepsilon}}^p) : \mathbb{C} : (\underline{\underline{\varepsilon}} - \underline{\underline{\varepsilon}}^p) + W^\gamma(\gamma^p) \tag{12}$$

$\underline{\underline{\varepsilon}}^p$ denotes the plastic strain tensor and γ^p represents the scalar internal variable for isotropic hardening. The set of internal variables can be written in the symbolic form: $\beta = (\underline{\underline{\varepsilon}}^p, \gamma^p)$. $\mathbb{C}$ is the elastic stiffness tensor of the clay matrix which is assumed isotropic: $\mathbb{C} = 3k\mathbb{J} + 2\mu\mathbb{K}$. The positive scalars k and μ are the elastic bulk and shear moduli, respectively; $\mathbb{J}$ and $\mathbb{K}$ the spherical and deviatoric operators, respectively. $\mathbb{J} = \frac{1}{3}\underline{\underline{1}} \otimes \underline{\underline{1}}$ and $\mathbb{K} = \mathbb{I} - \mathbb{J}$. The terms $\underline{\underline{1}}$ and $\mathbb{I}$ denote the second and fourth order symmetric identity tensor, respectively.

The state laws are obtained by standard derivation of the free energy with respect to the associated internal variables:

$$\underline{\underline{\sigma}}(\underline{\underline{\varepsilon}}, \beta) = \frac{\partial W}{\partial \underline{\underline{\varepsilon}}} = \mathbb{C} : (\underline{\underline{\varepsilon}} - \underline{\underline{\varepsilon}}^p) \tag{13}$$

$$F^p(\underline{\underline{\varepsilon}}, \beta) = -\frac{\partial W}{\partial \underline{\underline{\varepsilon}}^p} = \underline{\underline{\sigma}} \tag{14}$$

$$F^\gamma(\underline{\underline{\varepsilon}}, \beta) = -\frac{\partial W}{\partial \gamma^p} = -\frac{\partial W^\gamma}{\partial \gamma^p} = -\alpha^p(\gamma^p) \tag{15}$$

α^p is the thermodynamical force associated to the hardening variable γ^p. As the mechanical behavior of the clay matrix prior to failure state is generally not elastic, an elastic perfect plastic model is not suitable. An appropriate plastic hardening law is needed. In the present model, the plastic hardening process is described by the variation of α^p from its initial threshold α_0^p (at the elastic limit state) to the ultimate value α_m^p when the failure state is reached. The evolution law of α^p is experimentally determined and the following exponential form is here adopted:

$$\alpha^p(\gamma^p) = \alpha_m^p - (\alpha_m^p - \alpha_0^p)e^{-b\gamma^p} \tag{16}$$

The parameter b controls the kinetics of the evolution of plastic hardening. Taking into account the proposed hardening law, the yield function is expressed as follows:

$$f(F^{\mathrm{p}}, F^{\gamma}, \gamma^{\mathrm{p}}) = f(\underline{\underline{\sigma}}, \gamma^{\mathrm{p}}) = q + \alpha^{\mathrm{p}}(\gamma^{\mathrm{p}})(p - c_p) \tag{17}$$

The parameter c_p corresponds to hydrostatic tensile strength related to material cohesion. We can see that the thermodynamic force α^{p} physically represents the current mobilized frictional coefficient of clay matrix. As in the classical Drucker–Drucker approach, the yield surface defined by (17) depends on two basic stress invariants only, namely the mean stress $p = \mathrm{tr}(\underline{\underline{\sigma}})/3$ and the equivalent stress $q = \sqrt{\frac{3}{2}\underline{\underline{s}} : \underline{\underline{s}}}$, s being the deviatoric stress tensor. It is useful to point out that the plastic behavior of geomaterials in general loading condition also depends on the third stress invariant, the Lode angle. Keeping in mind that the main topic of the work is to develop a nonlinear homogenization method for heterogeneous geomaterials, the local behavior of constituent is kept as simple as possible. For this purpose and for the sake of simplicity, the effect of Lode angle is not taken into account in the local plastic model for the clay matrix. However, it is easy to improve the proposed model by introducing an additional term in the yield function depending on the Lode angle. Further, the macroscopic behavior of the argillite depends not only on the behavior of the clay matrix, but also on the damage behavior of calcite grains. The damage behavior is sensitive to loading path, and for example exhibits a dissymmetric behavior in tension and compression. Therefore, the macroscopic response of the homogenized argillite will also depend on loading path orientation. This reduces in some way the consequence of the simplification made on the local plastic model for the clay matrix.

For most geomaterials, the plastic flow (given by the plastic potential) does not comply with the normality rule. Plastic volumetric strain generally exhibits a transition from compressibility regime to dilation according to loading path. Therefore, for the flow rule we need to introduce this plastic potential, proposed in the form:

$$F(\underline{\underline{\sigma}}, \gamma^{\mathrm{p}}) = q + \beta^{\mathrm{p}}(\gamma^{\mathrm{p}})p \tag{18}$$

The coefficient β^{p} controls the rate of plastic volumetric strain; we have dilatancy for $\beta^{\mathrm{p}} > 0$ and compressibility for $\beta^{\mathrm{p}} \leqslant 0$. As the volumetric strain rate generally varies with plastic deformation history, it is assumed that the coefficient β^{p} is a function of the plastic hardening variable; that is

$$\beta^{\mathrm{p}}(\gamma^{\mathrm{p}}) = \beta^{\mathrm{p}}_m - (\beta^{\mathrm{p}}_m - \beta^{\mathrm{p}}_0)\mathrm{e}^{-b'\gamma^{\mathrm{p}}} \tag{19}$$

in which β^{p}_m and β^{p}_0 are, respectively, the initial and final dilatancy parameter.

The non-associated plastic flow rule is expressed as follows:

$$\underline{\underline{\dot{\varepsilon}}}^{\mathrm{p}} = \dot{\gamma}\frac{\partial F}{\partial \underline{\underline{\sigma}}} = \dot{\gamma}\left(\frac{\beta^{\mathrm{p}}}{3}\underline{\underline{1}} + \sqrt{\frac{3}{2}}\frac{\underline{\underline{s}}}{\sqrt{\underline{\underline{s}} : \underline{\underline{s}}}}\right) \tag{20}$$

As a deviatoric plastic mechanism is of concerns here, the plastic hardening variable γ^{p} of frictional materials is classically chosen as the generalized plastic distortion defined by

$$\dot{\gamma^{\mathrm{p}}} = \sqrt{\frac{2}{3}\mathrm{dev}(\underline{\underline{\dot{\varepsilon}}}^{\mathrm{p}}) : \mathrm{dev}\left(\underline{\underline{\dot{\varepsilon}}}^{\mathrm{p}}\right)} \tag{21}$$

$$= \dot{\gamma}\sqrt{\frac{2}{3}\mathrm{dev}\left(\frac{\partial F}{\partial \underline{\underline{\sigma}}}\right) : \mathrm{dev}\left(\frac{\partial F}{\partial \underline{\underline{\sigma}}}\right)} = \dot{\gamma} \tag{22}$$

where $\mathrm{dev}(\underline{\underline{\dot{\varepsilon}}}^{\mathrm{p}})$ is the deviatoric part of $\underline{\underline{\dot{\varepsilon}}}^{\mathrm{p}}$. By calculating the derivatives of yield function to stresses, the plastic flow rule can be written as

$$\begin{cases} \underline{\underline{\dot{\varepsilon}}}^{\mathrm{p}} = \dot{\gamma}\dfrac{\partial F}{\partial \underline{\underline{\sigma}}} = \dot{\gamma}\left(\dfrac{\beta^{\mathrm{p}}}{3}\underline{\underline{1}} + \sqrt{\dfrac{3}{2}}\dfrac{\underline{\underline{s}}}{\sqrt{\underline{\underline{s}} : \underline{\underline{s}}}}\right) \\ \dot{\gamma^{\mathrm{p}}} = \dot{\gamma} \\ \dot{\gamma} = 0 \quad \text{if } f(\underline{\underline{\sigma}}, \gamma^{\mathrm{p}}) \leqslant 0,\ \dot{f}(\underline{\underline{\sigma}}, \gamma^{\mathrm{p}}) < 0 \\ \dot{\gamma} > 0 \quad \text{if } f(\underline{\underline{\sigma}}, \gamma^{\mathrm{p}}) = 0,\ \dot{f}(\underline{\underline{\sigma}}, \gamma^{\mathrm{p}}) = 0 \end{cases} \tag{23}$$

The plastic multiplier $\dot{\gamma}$ is determined by using the plastic consistency condition. The rate form of the constitutive equations, obtained by time derivation of the stress tensor $\underline{\underline{\sigma}}$, takes then the following form:

$$\dot{\underline{\underline{\sigma}}} = \mathbb{L} : \dot{\underline{\underline{\varepsilon}}} \tag{24}$$

where the tangent modulus $\mathbb{L}$ is computed by using the standard consistency condition and the relations (17) and (18):

$$\mathbb{L}_0 = \begin{cases} \mathbb{C} & \text{if } f(\underline{\underline{\sigma}}, \gamma^p) \leqslant 0,\ \dot{f}(\underline{\underline{\sigma}}, \gamma^p) < 0 \\ \mathbb{C} - \dfrac{\mathbb{C} : \dfrac{\partial F}{\partial \underline{\underline{\sigma}}} \otimes \dfrac{\partial f}{\partial \underline{\underline{\sigma}}} : \mathbb{C}}{h} & \text{if } f(\underline{\underline{\sigma}}, \gamma^p) = 0,\ \dot{f}(\underline{\underline{\sigma}}, \gamma^p) = 0 \end{cases} \tag{25}$$

$$\text{with, } h = \frac{\partial f}{\partial \underline{\underline{\sigma}}} : \mathbb{C} : \frac{\partial F}{\partial \underline{\underline{\sigma}}} - \frac{\partial f}{\partial \gamma^p} \tag{26}$$

In case of isotropic hardening and by making use of relations (17) and (18), the following expression is obtained:

$$\mathbb{L}_0 = 3k_1\mathbb{J} + 2k_2\mathbb{K} - 2k_3\underline{\underline{n}} \otimes \underline{\underline{1}} - 2k_4\underline{\underline{1}} \otimes \underline{\underline{n}} - 2k_5\underline{\underline{n}} \otimes \underline{\underline{n}}$$

with the parameters k_i, $i = 1, \ldots, 5$, given by

$$k_1 = k\left(1 - \frac{\alpha^p\beta^p k}{h}\right), \quad k_2 = \mu, \quad k_3 = \frac{\mu}{h}\sqrt{\frac{2}{3}}\alpha^p k, \quad k_4 = \frac{\mu}{h}\sqrt{\frac{2}{3}}\beta^p k, \quad k_5 = \frac{6\mu}{h}$$

The other quantities read: $\underline{\underline{n}} = \frac{\underline{\underline{s}}}{\sqrt{\underline{\underline{s}} : \underline{\underline{s}}}}$ and scalar $h = \alpha^p\beta^p k + 3\mu - (p - c_p)\frac{\mathrm{d}\alpha^p}{\mathrm{d}\gamma^p}$.

4.2. Elastic unilateral damage behavior of the calcite phase

In this subsection we propose to formulate an isotropic damage model for calcite phase, accounting for unilateral effects due to microcracks closure. It is well known that the mechanical response of a microcracked medium strongly depends on the opening and closure status of the existing defects in the material. It should be first noted that the consideration of the unilateral effects in Continuum Damage Mechanics (CDM) framework still constitutes a challenging task. The main difficulty lies in the necessity to predict both continuous response of the material and partial or total recovery of the elastic constants during the microcracks closure process. We propose here a mathematically rigorous and physically-motivated model based on micromechanical considerations.

It is assumed here that the nonlinear behavior is caused by the growth of microcracks. Since the microcracks are expected to be randomly oriented, the damage state is represented by a positive scalar variable d which corresponds to the microcracks density parameter (see Budiansky and O'Connell, 1976) in the calcite grains. As classically, the elastic damage behavior is characterized by the existence of a thermodynamical potential (free energy) which depends on the internal variable d and the strain tensor $\underline{\underline{\varepsilon}}$:

$$W(\underline{\underline{\varepsilon}}, d) = \tfrac{1}{2}\underline{\underline{\varepsilon}} : \mathbb{C}(d) : \underline{\underline{\varepsilon}} \tag{27}$$

where $\mathbb{C}(d)$ represents the isotropic stiffness tensor of the damaged grains. This potential must be continuously differentiable with respect to the strain tensor to assure the existence of the state laws which give: the stress tensor $\underline{\underline{\sigma}}$ $(\underline{\underline{\varepsilon}}, d)$

$$\underline{\underline{\sigma}}(\underline{\underline{\varepsilon}}, d) = \frac{\partial W}{\partial \underline{\underline{\varepsilon}}}(\underline{\underline{\varepsilon}}, d) \tag{28}$$

and the thermodynamical force $F^d(\underline{\underline{\varepsilon}}, d)$ associated to the damage variable:

$$F^d(\underline{\underline{\varepsilon}}, d) = -\frac{\partial W}{\partial d}(\underline{\underline{\varepsilon}}, d) \tag{29}$$

For modeling the unilateral damage of the calcite the stiffness tensor is separately described when the microcracks are opened or closed by $\mathbb{C}^o(d)$ and $\mathbb{C}^f(d)$, respectively. The simplest partition of the strain space into

two half-spaces is provided by a hyperplan g which depends on $\underline{\underline{\varepsilon}}$. It is assumed that the opening and closure state does not depend on the microcracks density parameter but only on the strain state. Therefore, the microcracks are opened if $g(\underline{\underline{\varepsilon}}) > 0$ and closed if $g(\underline{\underline{\varepsilon}}) \leqslant 0$. The isotropic stiffness tensor of the damaged grains takes then the following form:

$$\mathbb{C}(d) = \begin{cases} \mathbb{C}^o(d) = 3K^o(d)\mathbb{J} + 2G^o(d)\mathbb{K} & \text{if } g(\underline{\underline{\varepsilon}}) > 0 \\ \mathbb{C}^f(d) = 3K^f(d)\mathbb{J} + 2G^f(d)\mathbb{K} & \text{if } g(\underline{\underline{\varepsilon}}) \leqslant 0 \end{cases} \tag{30}$$

(K^o, G^o) and (K^f, G^f) moduli represent the compressibility and shear moduli for opened and closed microcracks, respectively. Since the thermodynamical potential has to be continuously differentiable, (K^o, G^o) and (K^f, G^f) must fulfill some conditions. Curnier et al. (1995) (see also Welemane and Cormery, 2003) have demonstrated that the elastic energy function W is C^1 continuous if and only if:

$$[\mathbb{C}(d)] = \mathbb{C}^o(d) - \mathbb{C}^f(d) = s(d)\frac{\partial g}{\partial \underline{\underline{\varepsilon}}}(\underline{\underline{\varepsilon}}) \otimes \frac{\partial g}{\partial \underline{\underline{\varepsilon}}}(\underline{\underline{\varepsilon}}), \quad \forall \underline{\underline{\varepsilon}} | g(\underline{\underline{\varepsilon}}) = 0 \tag{31}$$

where s is a continuous scalar valued function depending on d. Using (30), we obtain the following jump:

$$[\mathbb{C}(d)] = 3[K^o(d) - K^f(d)]\mathbb{J} + 2[G^o(d) - G^f(d)]\mathbb{K} \tag{32}$$

The jump $[\mathbb{C}(d)]$ of the stiffness tensor must be singular and in fact of rank one to satisfy the condition (31) (Curnier et al., 1995). This condition is fulfilled if all determinants of second order obtained from a voigt representation of $[\mathbb{C}(d)]$ are canceled, that is

$$\forall d, \quad G^o(d) = G^f(d) \tag{33}$$

The continuity of W is then obtained if the shear moduli does not depend on the microcracks state. It follows for the shear moduli of the damaged material that $G(d) = G^o(d) = G^f(d)$.

It can be noted that no mathematical conditions are imposed on the compressibility moduli. According to experimental observations on the progressive closure effects of microcracks (Sibai et al., 2003), we assume as well that the compressibility modulus, when the microcracks are closed takes the initial value K_0 of the sound material. Therefore, the modulus restitution condition reads:

$$K^f(d) = K_0 \tag{34}$$

and we will denote $K^o(d) = K(d)$.

At this level of development, it remains to precise the expression of the function g which defines the microcracks closure criterion. In view of (32) and (33), the tensor $[\mathbb{C}(d)]$ is written in the form:

$$[\mathbb{C}(d)] = 3[K^o(d) - K^f(d)]\mathbb{J} = [K^o(d) - K^f(d)]\underline{\underline{1}} \otimes \underline{\underline{1}} \tag{35}$$

Comparing (31) and (35), it follows that the closure/opening criterion reads:

$$g(\underline{\underline{\varepsilon}}) = \mathrm{tr}(\underline{\underline{\varepsilon}}) = \underline{0} \tag{36}$$

It must be emphasized that the simplicity of the microcrack opening–closure transition criterion is due to the isotropy of the damage. In the case of a anisotropic damage, the methodology followed in this work would lead to a more complex criterion which depends in particular on the microcracks orientation.

Finally, the thermodynamical potential takes the following form:

$$W(\underline{\underline{\varepsilon}}, d) = \frac{1}{2}\underline{\underline{\varepsilon}} : \mathbb{C}(d) : \underline{\underline{\varepsilon}}, \quad \mathbb{C}(d) = \begin{cases} 3K(d)\mathbb{J} + 2G(d)\mathbb{K} & \text{if } \mathrm{tr}(\underline{\underline{\varepsilon}}) > 0 \\ 3K_0\mathbb{J} + 2G(d)\mathbb{K} & \text{if } \mathrm{tr}(\underline{\underline{\varepsilon}}) \leqslant 0 \end{cases} \tag{37}$$

In order to provide a physical basis to the damage model, we consider for $K(d)$ and $G(d)$ micromechanical results established by Ponte-Castañeda and Willis (1995) for microcracked media. These results have the interest of taking into account, not only the interactions between microcracks, but also their spatial distribution. For this purpose, two tensors describing the microcracks shape and their ellipsoidal spatial distribution, respectively, must be considered. For a randomly oriented penny-shaped microcracks with a spherical spatial distribution, one gets (Ponte-Castañeda and Willis, 1995):

$$K(d) = K_0\left(1 - \frac{48(1-v_0^2)d}{27(1-2v_0) + 16d(1+v_0)^2}\right) \tag{38}$$

$$G(d) = G_0\left(1 - \frac{480(1-v_0)(5-v_0)d}{675(2-v_0) + 64d(4-5v_0)(5-v_0)}\right) \tag{39}$$

where v_0 is the Poisson ratio of the undamaged grains..

Now, following Marigo (1985), let us introduce the yield function f in a form which depends on the thermodynamical force F^d and on the damage variable d:

$$f(F^d, d) = F^d - H(d) \tag{40}$$

H is a scalar strictly positive function:

$$\begin{cases} H(d) = H_0(1+\eta d) \\ \text{with } H_0 > 0 \text{ and } \eta > 0 \end{cases} \tag{41}$$

Assuming the standard normality rule, one has:

$$\begin{cases} \dot{d} = \dot{\gamma}\frac{\partial f}{\partial F^d}(F^d, d) = \dot{\gamma} \\ \dot{\gamma} = 0 \quad \text{if } f(F^d, d) \leqslant 0, \dot{f}(F^d, d) < 0 \\ \dot{\gamma} > 0 \quad \text{if } f(F^d, d) = 0, \dot{f}(F^d, d) = 0 \end{cases} \tag{42}$$

in which the damage multiplier $\dot{\gamma}$ is given by the consistency condition. Reporting this evolution law in the rate form of the stress tensor one gets the incremental formulation of the elastic damage law:

$$\dot{\underline{\underline{\sigma}}} = \mathbb{L} : \dot{\underline{\underline{\varepsilon}}} \tag{43}$$

with the tangent operator $\mathbb{L}$ given by the following expression:

$$\mathbb{L}_1 = \begin{cases} \mathbb{C}(d) & \text{if } f(F^d, d) \leqslant 0, \dot{f}(F^d, d) < 0 \\ \mathbb{C}(d) - \dfrac{\frac{\partial F^d}{\partial \underline{\underline{\varepsilon}}} \otimes \frac{\partial F^d}{\partial \underline{\underline{\varepsilon}}}}{h} & \text{if } f(F^d, d) = 0, \dot{f}(F^d, d) = 0 \end{cases} \tag{44}$$

in (44), tensor $\mathbb{C}(d)$ is given by (37) and $h = H_0\eta - \frac{\partial F^d}{\partial d}$.

Combining (29) and (37) and in case of a damage evolution, we obtain the final expressions:

$$\mathbb{L}_1 = 3k_1\mathbb{J} + 2k_2\mathbb{K} - 2k_3(\underline{\underline{1}} \otimes \underline{\underline{e}} + \underline{\underline{e}} \otimes \underline{\underline{1}}) - 2k_4\underline{\underline{e}} \otimes \underline{\underline{e}} \tag{45}$$

$k_2 = G(d)$, $k_4 = \frac{2(G'(d))^2}{h}$,

$$\begin{cases} k_1 = \left(K(d) - \dfrac{(K'(d)\,\mathrm{tr}\,\underline{\underline{\varepsilon}})^2}{h}\right) & \text{and} \quad k_3 = \left(K(d) - \dfrac{G'(d)K'(d)}{h}\right) & \text{if } \mathrm{tr}(\underline{\underline{\varepsilon}}) > 0 \\ k_1 = K_0 & \text{and} \quad k_3 = 0 & \text{if } \mathrm{tr}(\underline{\underline{\varepsilon}}) \leqslant 0 \end{cases} \tag{46}$$

$h = H_0\eta + K''(d)\,\mathrm{tr}\,\underline{\underline{\varepsilon}}\underline{\underline{1}} + G''(d)\,\underline{\underline{e}}$ where $K''(d)$ and $G''(d)$ are the second derivative of $K(d)$ and $G(d)$, respectively, whereas $K'(d)$ and $G'(d)$ are the first derivative of $K(d)$ and $G(d)$, respectively.

5. Implementation and numerical validation of the model

5.1. Local integration of the micromechanical model

This integration is done for each integration point (or Gauss point) of the elements.

We still consider a three phases material whose r.v.e. is subjected to an uniform macroscopic strain $\underline{\underline{E}}_{n+1} = \underline{\underline{E}}_n + \Delta\underline{\underline{E}}$ at the step $(n+1)$. We adopt the resolution scheme described as follows.

Let us denote $\Delta\overline{\underline{\underline{\varepsilon}}}_r^i$, the estimates of the strain increment average at the increment (i) for the phase r.

(1) We initialize the average of the deformation increment to the macroscopic deformation:

$$\Delta\underline{\underline{\varepsilon}}_1^0 := \Delta\underline{\underline{E}} \tag{47}$$

$$\Delta\underline{\underline{\varepsilon}}_2^0 := \Delta\underline{\underline{E}} \tag{48}$$

(2) At the iteration i, the values of $\Delta\underline{\underline{\varepsilon}}_1^i$ and $\Delta\underline{\underline{\varepsilon}}_2^i$ are known, and we are able to determine the tangent moduli $\mathbb{L}_1^i$ and $\mathbb{L}_2^i$ with the help of the local integration scheme in the phases 1 and 2.

(3) The average strain in the matrix is obtained by

$$\Delta\underline{\underline{\varepsilon}}_0^i := \frac{\Delta\underline{\underline{E}} - f_1\Delta\underline{\underline{\varepsilon}}_1^i - f_2\Delta\underline{\underline{\varepsilon}}_2^i}{1-f_1-f_2} \tag{49}$$

(4) We can thus determine the tangent moduli $\mathbb{L}_0^i$ with the help of the local integration scheme of the phase 0.

(5) Hill tensor $\mathbb{P}_I^0$ is evaluated by numerical integration.

(6) Calculation of the tensors $\mathbb{T}_1^i$ and $\mathbb{T}_2^i$:

$$\mathbb{T}_1^i := \left[\mathbb{I} + \mathbb{P}_I^0 : (\mathbb{L}_1^i - \mathbb{L}_0^i)\right]^{-1} \tag{50}$$

$$\mathbb{T}_2^i := \left[\mathbb{I} + \mathbb{P}_I^0 : (\mathbb{L}_2^i - \mathbb{L}_0^i)\right]^{-1} \tag{51}$$

(7) It is thus possible to determine the incremental localization tensor $\mathbb{A}_r^i$ for each phase with the expression (9):

$$\mathbb{A}_0^i := \left[f_0\mathbb{I} + f_1\mathbb{T}_1^i + f_2\mathbb{T}_2^i\right]^{-1} \tag{52}$$

$$\mathbb{A}_1^i := \mathbb{T}_1^i : \mathbb{A}_0^i \tag{53}$$

$$\mathbb{A}_2^i := \mathbb{T}_2^i : \mathbb{A}_0^i \tag{54}$$

(8) We verify after that the compatibility of the average strains for the phases (1) and (2) and perform the calculations of corresponding error R:

$$\underline{\underline{R}}_1^i := \mathbb{A}_1^i : \Delta\underline{\underline{E}} - \Delta\underline{\underline{\varepsilon}}_1^i \tag{55}$$

$$\underline{\underline{R}}_2^i := \mathbb{A}_2^i : \Delta\underline{\underline{E}} - \Delta\underline{\underline{\varepsilon}}_2^i \tag{56}$$

If $\|\underline{\underline{R}}_1^i\| <$ tolerance 1 and if $\|\underline{\underline{R}}_2^i\| <$ tolerance 2, then the solution is obtained. Else, we make a new iteration with:

$$\Delta\underline{\underline{\varepsilon}}_1^{i+1} := \Delta\underline{\underline{\varepsilon}}_1^i + \underline{\underline{R}}_1^i \tag{57}$$

$$\Delta\underline{\underline{\varepsilon}}_2^{i+1} := \Delta\underline{\underline{\varepsilon}}_2^i + \underline{\underline{R}}_2^i \tag{58}$$

until the convergence is obtained.

(9) We determine, with the Mori–Tanaka scheme, the macroscopic tangent tensor:

$$\mathbb{L}^{\text{hom}} := [f_0\mathbb{L}_0 + f_1\mathbb{L}_1 : \mathbb{T}_1 + f_2\mathbb{L}_2 : \mathbb{T}_2] : \mathbb{A}_0 \tag{59}$$

$$\Delta\underline{\underline{\Sigma}}_{n+1} := \mathbb{L}^{\text{hom}} : \Delta\underline{\underline{E}}_{n+1} \tag{60}$$

5.2. Comparison with unit cell (finite element) calculation

In order to provide a first validation of the micromechanical approach, we present in this section some comparisons of its predictions with reference solutions obtained by Finite Element (FE) calculations. For this, we consider the same assumptions on the local constituents in both homogenization and FE calculations.

The FE reference solution is obtained by considering an unit cell.[2] As illustrated in Fig. 7, space is supposed filled by prisms with hexagonal basis which represent the matrix, each prism being reinforced by a spherical

[2] In fact, this unit cell calculation corresponds rigorously to periodic composites. However, it is generally noted that the comparison is meaningful for low or moderate volume fraction of particles.

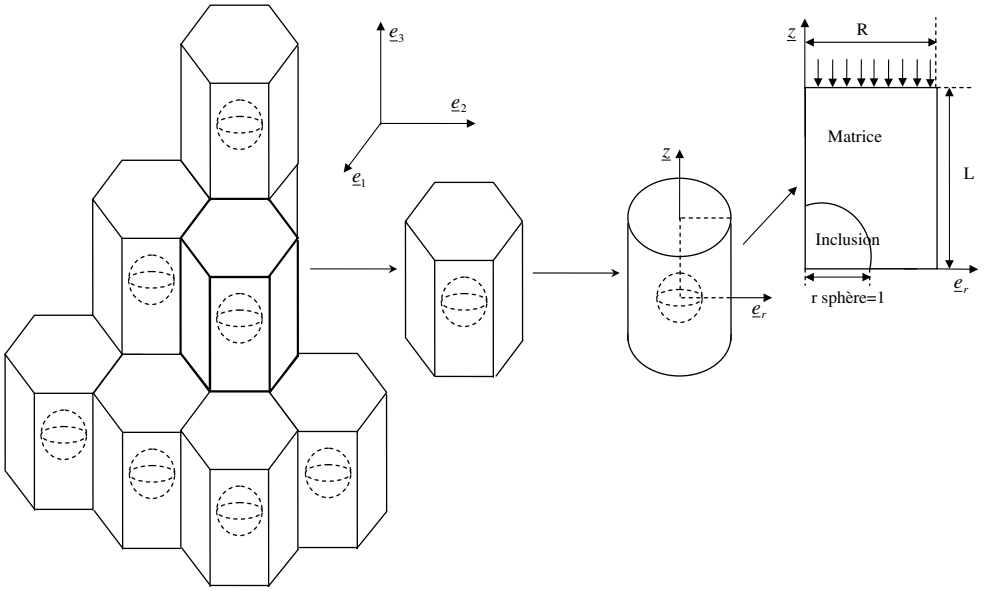

Fig. 7. A hexagonal periodic array of sphere-reinforced reduction to a 2D axisymmetric unit cell.

inclusion in its center. In order to take advantage of symmetry, the 3D unit cells are approximated by cylinders to allow axisymmetric computations. The boundary conditions are the following:

- $U_3(r,0) = 0,\ 0 < r < R$
- $U_3(r,L) = \overline{U}_3,\ 0 < r < R$
- $U_1(0,z) = 0,\ 0 < z < L$
- $U_1(R,z) = \overline{U}_1,\ 0 < z < L$

The displacement on the top side $\overline{U}_3$ is prescribed gradually with time to reach the required strain at the end of the simulation. The unit cell, used in the simulation, is with 15% of reinforcements and has 963 CAX8R elements (8-node biquadratic axisymmetric quadrilaterals, with reduced integration) and contains 3002 nodes.

The chosen configuration corresponds to a two phase material, with spherical elastic inclusions embedded in an elastoplastic matrix. In the numerical simulation, as already indicated, the model parameters used are the same both in the micromechanical approach and in the FE calculations. Nevertheless, parameters are chosen to obtain an homogenized behavior closed to the argillite one. The matrix behavior is described by the following parameters: $E_0 = 3$ GPa, $\nu_0 = 0.3$, $\alpha_0^{\mathrm{p}} = 0.4$, $\alpha_m^{\mathrm{p}} = 0.9$, $b = 400$, $\beta_0^{\mathrm{p}} = 0.1$, $\beta_m^{\mathrm{p}} = 0.8$, $b' = 400$ and $c_p = 14$. The elastic inclusion is described with the following parameters: $E_1 = 100$ GPa and $\nu_1 = 0.2$.

In Fig. 8, we present for an uniaxial compression test, the comparison between the model prediction and the periodic homogenization. Unfortunately, it appears that the predicted response is too stiff compared with the FE solution. This observation is similar to the one that has been reported by Chaboche and Kanouté (2005) and Doghri and Ouaar (2003) in the context of metals plasticity.

5.3. Isotropization procedure and validation

In the case of a Von Mises matrix, Doghri and Ouaar (2003) have shown that a way to improve the micromechanical results consists in considering an isotropic version in which the Eshelby tensor is evaluated by using an isotropic approximation of the tangent operator associated to the clay matrix ("$S^E - Iso$" procedure).

For this purpose, we consider the general method proposed by Bornert et al. (2001) and which is applicable to any fourth order tensor:

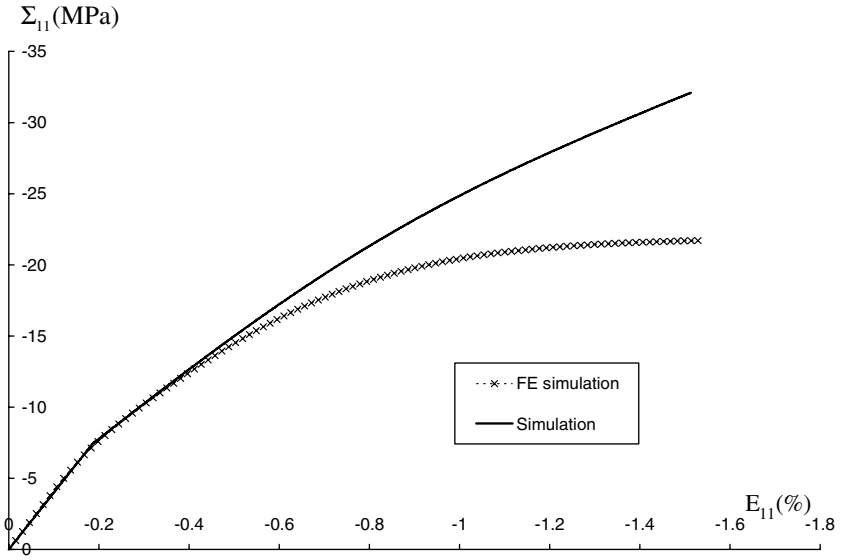

Fig. 8. Uniaxial compression test: comparison of the incremental formulation and the reference FE solution.

$$\mathbb{L}_0^{\text{iso}} = (\mathbb{J} :: \mathbb{L}_0)\mathbb{J} + \tfrac{1}{5}(\mathbb{K} :: \mathbb{L}_0)\mathbb{K} \tag{61}$$

Reporting expression (25) of $\mathbb{L}_0$ in (61), we obtain:

$$\mathbb{L}_0^{\text{iso}} = 3k_T\mathbb{J} + 2\mu_T\mathbb{K} \tag{62}$$

$$k_T = k\left(1 - \frac{k\alpha^{\text{p}}\beta^{\text{p}}}{h}\right) \quad \text{and} \quad \mu_T = \mu\left(1 - \frac{3\mu}{5h}\right)$$

$$\text{with,} \quad h = \alpha^{\text{p}}\beta^{\text{p}}k + 3\mu - (p - c_p)\frac{\mathrm{d}\alpha^{\text{p}}}{\mathrm{d}\gamma^{\text{p}}}$$

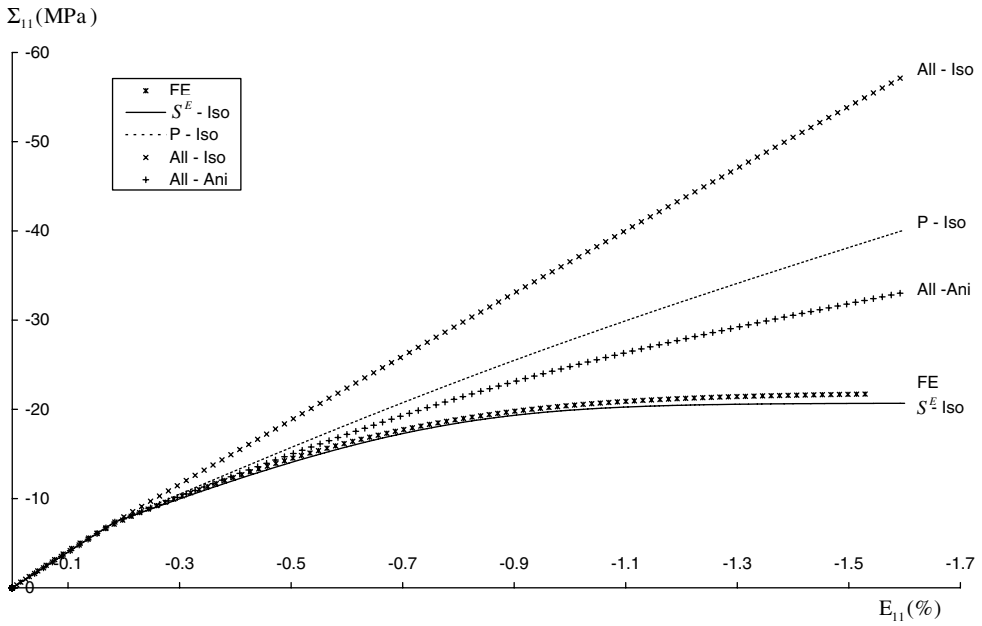

Fig. 9. Uniaxial compression test: comparisons between "$S^E - Iso$", "$P - Iso$", "$All - Iso$", and "$All - Ani$" procedures and the reference FE solution.

According to the assumption of isotropy and the fact that the grains are spherical, the Eshelby tensor is analytically evaluated and is expressed as

$$\mathbb{S}^E = \frac{3k_T}{3k_T + 4\mu_T}\mathbb{J} + \frac{6}{5}\frac{k_T + 2\mu_T}{3k_T + 4\mu_T}\mathbb{K} \tag{63}$$

At the step (5) of the algorithm described in Section 5.1, the Hill tensor is simply given by

$$\mathbb{P}^0_{I_r} = \mathbb{S}^E(\mathbb{L}^{\text{iso}}_0) : \mathbb{L}_0^{-1}, \quad r = 1, 2 \tag{64}$$

Other variants of the above procedure are possible: for example by using an isotropic extraction of the clay matrix tangent operator to compute the Hill tensor $\mathbb{P}^0_{I_r} = \mathbb{S}^E(\mathbb{L}^{\text{iso}}_0) : (\mathbb{L}^{\text{iso}}_0)^{-1}$, one obtains a procedure called here "$P - Iso$"; it is also possible to compute entirely the macro tangent operator by considering the isotropic operator $\mathbb{L}^{\text{iso}}_0$. This is called here "$All - Iso$". It must be noted that the last procedure give non-physical results because the macro tangent become symmetric, what it is not desirable for most geomaterials.

In the case of J_2 plasticity theory, Pierard and Doghri (2006) have demonstrated that the two last versions lead to too stiff predictions. For a Drucker–Prager matrix, the predictions of the different procedures and of the basic anisotropic procedure ("$All - Ani$") are compared in Fig. 9 to the FE calculations. It appears that the first isotropization procedure ("$S^E - Iso$") provides results in agreement with the FE ones and will be then adopted in the following.

Depth (m)	466.8	468.9	482.2
concentration	$f_0 = 51\%$	$f_0 = 34\%$	$f_0 = 60\%$
	$f_1 = 23\%$	$f_1 = 13\%$	$f_1 = 14\%$
	$f_2 = 26\%$	$f_2 = 53\%$	$f_2 = 26\%$
$E(MPa)$	8100	12200	8167
$E^{hom}(MPa)$	8173	12864	6647
ν	0.3	0.3	0.3
ν^{hom}	0.27	0.28	0.27

Fig. 10. Comparison between the homogenized moduli and experimental ones.

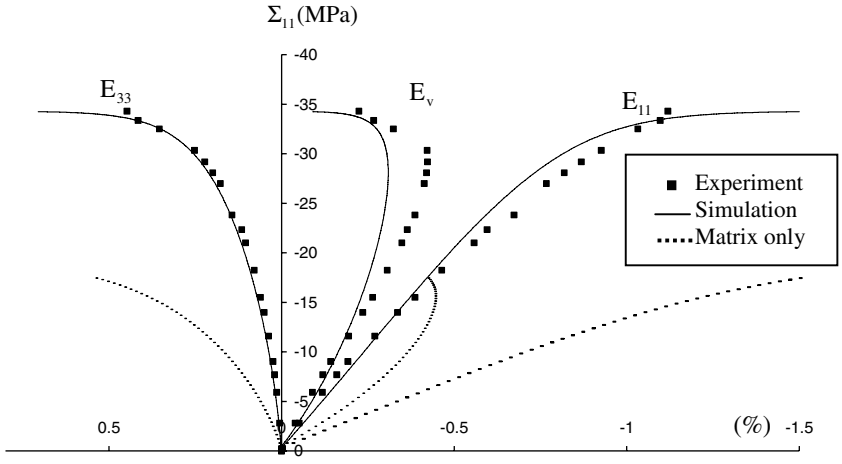

Fig. 11. Uniaxial compression, prof: 466.8 m, $f_0 = 51\%$, $f_1 = 26\%$, $f_2 = 23\%$.

6. Calibration and experimental validations of the micromechanical model

The purpose of this last part of the study is to evaluate the predictive capabilities of the proposed model and in particular its ability to reproduce the mechanical behavior of the argillite under various loading paths. It

	Phase (0) Clay	Phase (1) Calcite	Phase (2) Quartz
Elastic parameters	$E_0 = 3\text{GPa}$ $\nu_0 = 0.3$	$E_1 = 95\text{GPa}$ $\nu_1 = 0.27$	$E_2 = 101\text{GPa}$ $\nu_2 = 0.06$
plastic	$\alpha_0^p = 0.05$ $\alpha_m^p = 0.95$ $b = 300$ $\beta_0^p = -1.5$ $\beta_m^p = 0.3$ $b' = 400$ $c_p = 14$		
damaged		$h = 0.001$ $\eta = 150$	

Fig. 12. Parameters of the model.

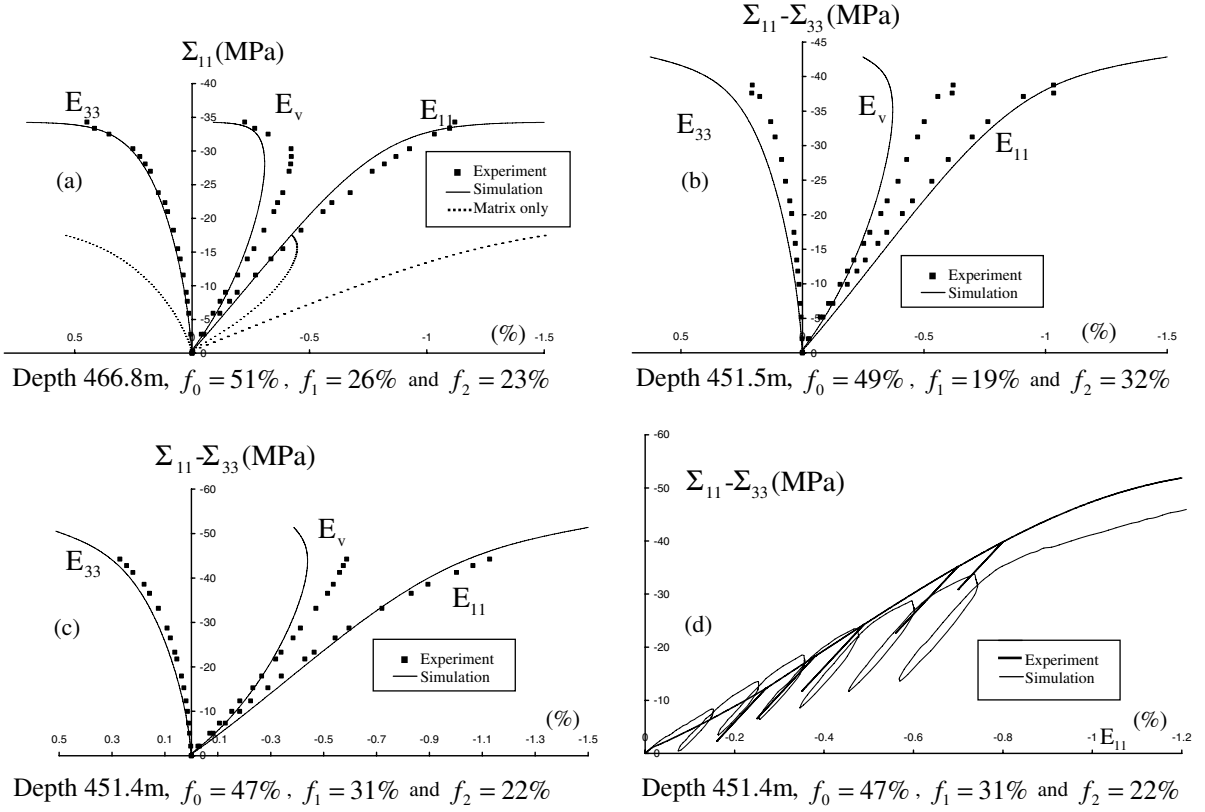

Fig. 13. Depth 1. Comparison between experiment and simulation: (a) Uniaxial compression test. (b) Triaxial compression test with 5 MPa confining pressure. (c) Triaxial compression test with 10 MPa confining pressure. (d) Loading and unloading in triaxial compression test with 10 MPa confining pressure.

must be first emphasized that in the following, only the version of the model based on the above isotropization procedure is considered.

6.1. Identification of the model parameters

A preliminary step is the determination of the model parameters: 6 elastic coefficients, 7 parameters involved in the plastic constituent of the materials, and 2 constants for the damage evolution in the calcite grains.

The elastic parameters associated with the calcite and quartz constituents are chosen according to the literature (Lide, 2004): $E_1 = 95$ GPa, $\nu_1 = 0.27$, $E_2 = 101$ GPa, and $\nu_2 = 0.06$. Unfortunately, the elastic coefficients of the clay matrix are unknown. Since the macroscopic elastic constants of the calcite and quartz phases are given and the ones of the argillite composite are known from experiments by Chiarelli et al. (2003), we use the linear homogenization scheme (Mori–Tanaka) to identify the appropriate values of elastic coefficients corresponding to the clay matrix. We obtain an average value of $E_0 = 3$ GPa for the elastic modulus and of $\nu_0 = 0.3$ for the Poisson ratio which are also in agreement with macroscopic modulus measured on samples at different depths (e.g., mineral compositions) (Fig. 10).

The identification of the other parameters for the local plastic and elastic damage behaviors has been performed by calibration on uniaxial compression test at the depth 466.8 m (Fig. 11). The retained values at the end of this procedure are summarized in Fig. 12.

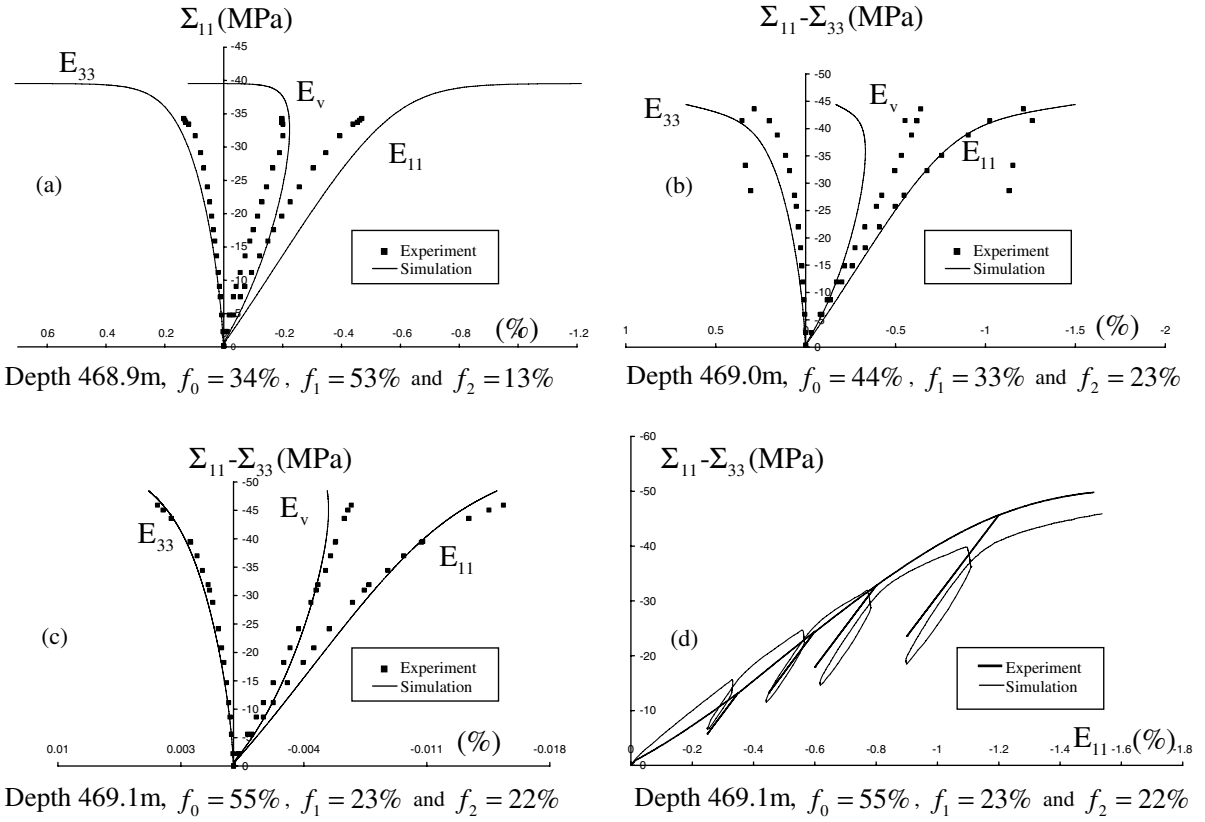

Fig. 14. Depth 2. Comparison between experiment and simulation: (a) Uniaxial compression test. (b) Triaxial compression test with 5 MPa confining pressure. (c) Triaxial compression test with 10 MPa confining pressure. (d) Loading and unloading in triaxial compression test with 10 MPa confining pressure.

6.2. Experimental validations

After the above calibration step, we propose to show the potentialities of the proposed model, keeping the same identified parameters on all tests (uniaxial and triaxial compression tests with 5 and 10 MPa confinement pressure, proportional compression tests, lateral extension tests). It is worth noticing that the considerations of these tests at different depths (451.4–466.8; 468.9–469.1; and 482.2 m), e.g., different mineral compositions, will provide a very complete evaluation of the model.

6.2.1. Triaxial compression tests

The comparisons of the macroscopic stress–strain curves and the experimental data are presented in Figs. 13, 14, and 15 for triaxial compression tests. These comparisons indicate a good general agreement between model's predictions and experiments including cyclic response of the materials. They provide a clear validation of the model for the study of the argillite. The simulations of unloading paths during the triaxial tests (Figs. 13, 14, and 15d) allow also to show the capability of the model to reproduce the deterioration of the macroscopic elastic properties of the material as observed in the experiments performed by Chiarelli et al. (2003).

It is important to note that, without any supplementary calibration, the model is able to reproduce tests corresponding to samples at different depths only by considering the appropriate (and measured) change in the mineral composition of the material. Another interesting advantage of the micromechanical model over purely phenomenological-based models is to provide predictions of the local fields at each macroscopic stress

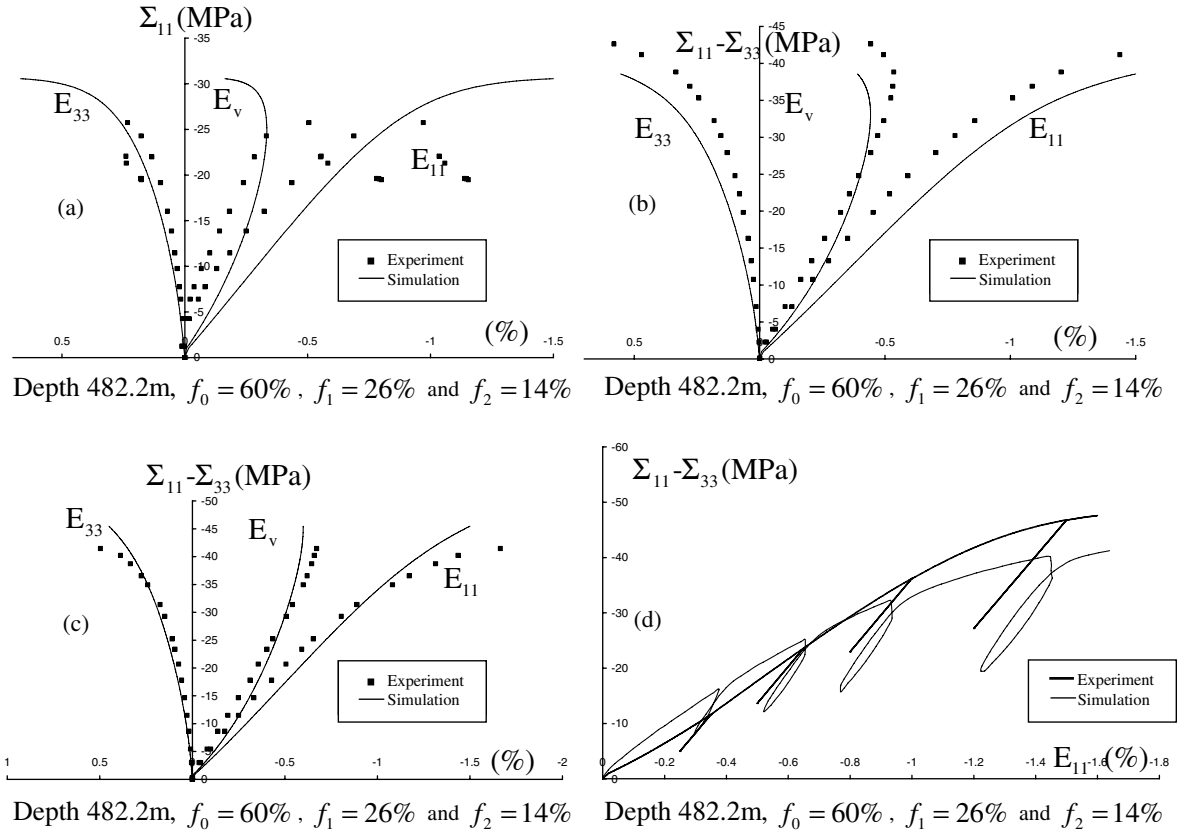

Fig. 15. Depth 3. Comparison between experiment and simulation: (a) Uniaxial compression test. (b) Triaxial compression test with 5 MPa confining pressure. (c) Triaxial compression test with 10 MPa confining pressure. (d) Loading and unloading in triaxial compression test with 10 MPa confining pressure.

level. As an example, we report on (Fig. 16a) the damage evolution in the calcite grains as a function of the macroscopic axial strain. The effect of this local damage on the elasticity of the calcite grains, as well as on the macroscopic parameters are shown in Figs. 16b and c. It is worth noticing that the amplitude of the decrease of the elastic moduli at local and macroscopic scales are strongly different. A possible consequence of the local damage is that it can favor a strong increase of the overall permeability although the macroscopic mechanical effect of damage is limited. This particular point still needs to be investigated in future works by following for instance Shao et al. (2005) and Dormieux et al. (2005).

Concerning the triaxial tests, we also show in Fig. 17 the variation of the local axial plastic strain and of the hardening function in the clay matrix.

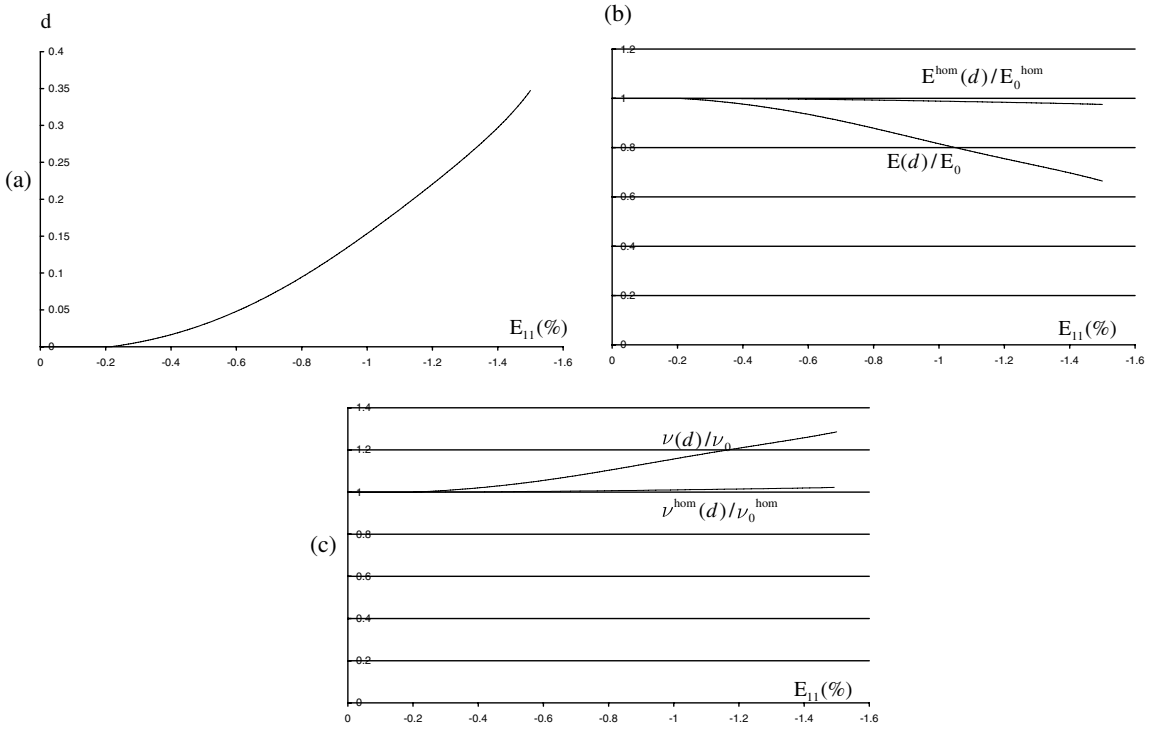

Fig. 16. Depth 451.4 m; $f_0 = 47\%$, $f_1 = 31\%$, and $f_2 = 22\%$. Triaxial compression test with 10 MPa confining pressure. (a) Variation of the local damage parameter with deviatoric stress. (b) Variation of the local Young modulus ratio as a function of lateral strain. (c) Variation of the local Poisson's ratio as a function of lateral strain.

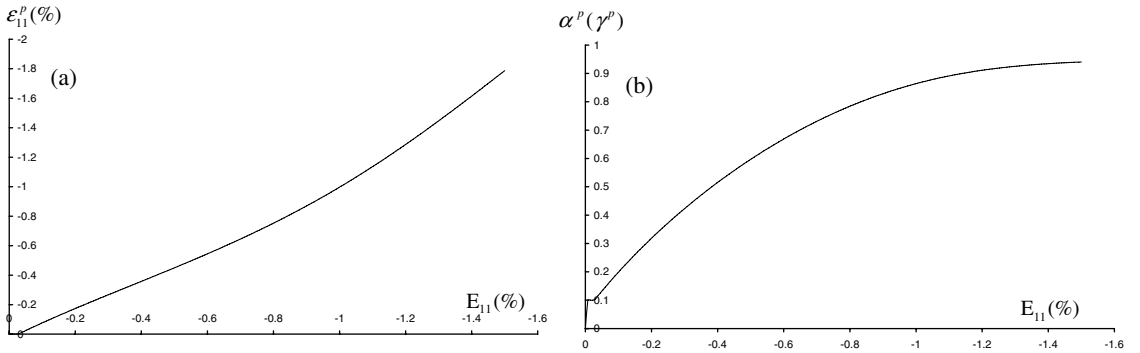

Fig. 17. Depth 451.4 m; $f_0 = 47\%$, $f_1 = 31\%$, and $f_2 = 22\%$. Triaxial compression test with 10 MPa confining pressure. (a) Variation of the local plastic strain as a function of lateral strain. (b) Variation of the hardening function as a function of lateral strain.

6.2.2. Proportional triaxial compression tests and lateral extension tests

In order to provide complementary validations of the model, we investigate now some other loading paths, namely the proportional triaxial compression and the lateral extension test which are important in various geomechanical applications. In a lateral extension test, the sample is first submitted to a hydrostatic stress and then the confining pressure is reduced while the axial stress is kept at a constant value. In a proportional test, the axial stress and confining pressure are simultaneously increased with a constant ratio $k = \frac{\Sigma_{11}}{\Sigma_{33}}$. Different values of k ($k = 5$, $k = 10$) are considered. The results, shown in Fig. 19 for proportional tests and in Fig. 18 for lateral extension tests, demonstrate that the predictions of the model on this loading path are in agreement with experimental stress–strain curves.

7. Conclusions

The coupled elastoplastic damage behavior of a cohesive frictional geomaterial, the Callovo-Oxfordian argillite, is investigated by the means of a nonlinear homogenization approach. The formulation of the model is carried out by means of a comprehensive analysis of the microstructure and the deformation mechanisms of the studied class of materials. It was shown that the argillite can be described as a three phase medium whose constituents are the clay matrix, the quartz grains, and the calcite grains. The clay matrix behaves as an elastoplastic material with possibility of a transition from plastic volumetric compressibility to dilatancy. In a first approximation and for the range of loading considered, the quartz grains have been considered as linear elastic. Observation of intragranular microcracks in calcite grains has motivated the modeling of these grains as elastic damage ones.

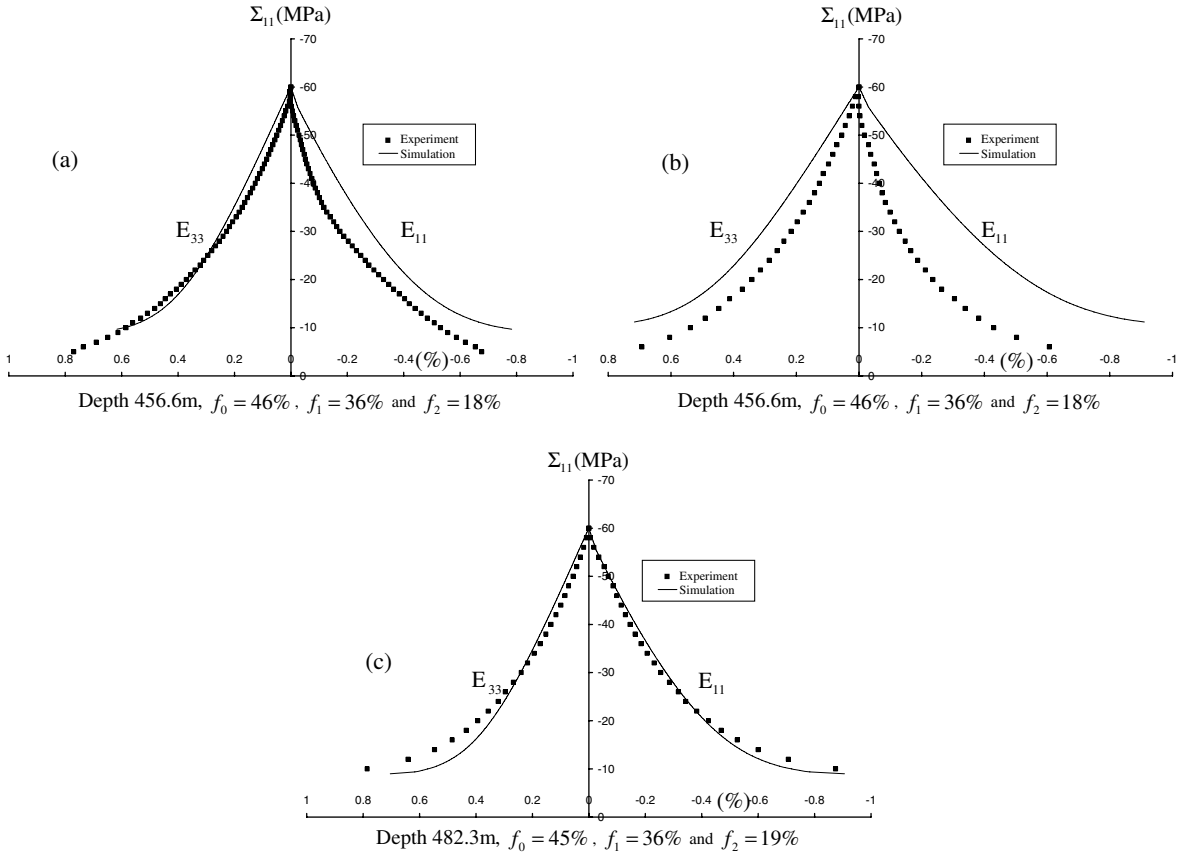

Fig. 18. Comparison between experiment and simulation of a lateral extension test with initial confining pressure of 60 MPa for three ranges of depths (a–c).

Based on the various experimental data and observations, we propose a specific model which takes the advantage of the well known incremental Hill-type homogenization procedure, classically applied to plastic behavior of heterogeneous metals. Our contribution is of three folds.

- An original formulation of the local behaviors of the argillites constituents. In particular, after a suitable derivation of a non-associated dilatant plastic model dedicated to the clay matrix, we propose a new elastic damage model which includes microcracks closure process (the so-called unilateral effects). This physically-based and mathematically coherent approach of elastic damage combines micromechanical considerations with the requirement of continuity of the mechanical response during the microcracks closure.
- An extension of the domain of applicability of the Hill-type incremental method of homogenization. Clearly enough, a novel aspect of the study is the consideration of plastic compressibility combined with an elastic damage behavior.

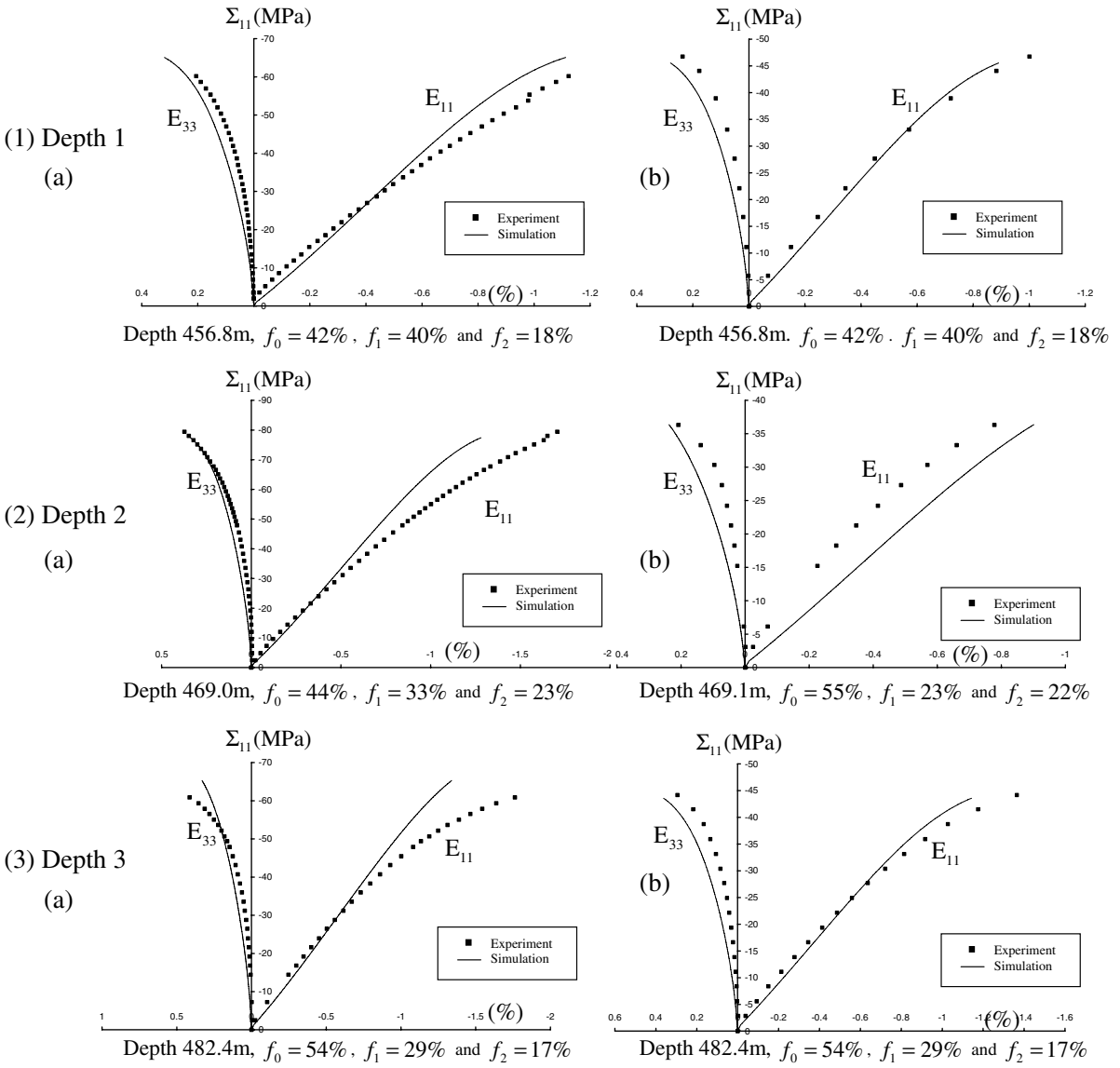

Fig. 19. Comparison between experiment and simulation of a proportional compression test with the stress ratio of (a) $k = 5$ and (b) $k = 10$ for three ranges of depths.

- The proposed micromechanical formulation of the plastic-damage coupled behavior enables the simulation of unloading and cyclic loadings. A large validation of the model is provided, by comparisons with Finite Element calculations on unit cell and by comparison with experimental data on various loading paths. More precisely, it is shown that, by considering a modified version of the original Hill method based on the use of an isotropization procedure of the local tangent operator (see for instance Chaboche and Kanouté, 2005; Doghri and Ouaar, 2003 in the case of metals plasticity), the model predictions are in satisfactory agreement with either the FE calculations and the experimental data. Moreover, the superiority of the micromechanical model over his phenomenological competitors is underlined by showing some predictions of local damage or local plastic deformations.

Among others, the ongoing developments mainly concern the extension of the model to the poroplastic damage behavior of the argillite material when it is saturated by fluid under pressure as in Dormieux et al. (2006) or in Shao et al. (2006).

Acknowledgments

The support from the French National Radioactive Waste Management Agency (ANDRA) is gratefully acknowledged. We thank more particularly Doctor K. Su from ANDRA.

References

Benveniste, Y., 1991. On diagonal and elastic symmetry of the approximate effective stiffness tensor of heterogeneous media. J. Mech. Phys. Solids 39 (7), 927–946.

Berveiller, M., Zaoui, A., 1979. An extension of the self-consistent scheme to plasticity flowing polycrystals. J. Mech. Phys. Solids 26, 325–344.

Bornert, M., Bretheau, T., Gilormini, P., 2001. Homogénéisation en mécanique des matériaux 1. Matériaux aléatoires élastiques et milieux périodiques. Hermes Sciences Europe Ltd.

Budiansky, B., O'Connell, R., 1976. Elastic moduli of a cracked solid. Int. J. Solids Struct. 12 (2), 81–97.

Chaboche, J.-L., Kanouté, P., 2005. On the capabilities of mean-field approaches for the description of plasticity in metal matrix composites. Int. J. Plasticity 21 (7), 1409–1434.

Chiarelli, A.-S., Shao, J.-F., Hoteit, N., 2003. Modeling of elastoplastic damage behavior of a claystone. Int. J. Plasticity 19, 23–45.

Conil, N., Djeran-Maigre, I., Cabrillac, R., Su, K., 2004. Poroplastic damage model for claystones. Appl. Clay Sci. 26, 473–487.

Curnier, A., He, Q.-C., Zysset, P., 1995. Conewise linear elastic materials. J. Elasticity 37, 1–38.

Doghri, I., Ouaar, A., 2003. Homogenization of two-phase elasto-plastic composite materials and structures: study of tangent operators, cyclic plasticity and numerical algorithms. Int. J. Solids Struct. 40 (7), 1681–1712.

Dormieux, L., Kondo, D., Ulm, F.-J., 2006. Microporomechanics. Wiley.

Dormieux, L., Kondo, D., 2005. Diffusive transport in disordered media application to the determination of the tortuosity and the permeability of cracked materials. In: Dormieux, L., Ulm, F.-J. (Eds.), Applied Micromechanics of Porous Media. CISM Courses and Lectures, vol. 480, pp. 83–106.

Drucker, D.-C., Prager, W., 1952. Soil mechanics and plastic analysis or limit design. Quart. Appl. Math. 10, 157–175.

Eshelby, J., 1957. The determination of the elastic field of an ellipsoidal inclusion, and related problems. Proc. R. Soc. Ser. A241, 376–396.

Gasc, R., 1999. Couplages hydromécaniques dans les argilites de l'est et les siltites du gard. Report ANDRA G3S B RP 0.G.3S. 99-002/A.

Gavazzi, A., Lagoudas, D., 1990. On the numerical evaluation of Eshelby's tensor and its application to elastoplastic fibrous composites. Comp. Mech. 7, 13–19.

Ghahremani, F., 1977. Numerical evaluation of the stresses and strains in ellipsoidal inclusions in an anisotropic elastic material. Mech. Res. Commun. 7, 8991.

Hill, R., 1965. Continuum micro-mechanics of elastoplastic polycrystals. J. Mech. Phys. Solids 13, 89–101.

Lide, D.-R., 2004. Handbook of Chemistry and Physics. CRC Press.

Marigo, J.-J., 1985. Modeling of brittle and fatigue damage for elastic material by growth of microvoids. Eng. Fract. Mech. 21 (4), 861–874.

Masson, R., Bornert, M., Suquet, P., Zaoui, A., 2000. An affine formulation for the prediction of the effective properties of nonlinear composites and polycrystals. J. Mech. Phys. Solids 48, 1203–1227.

Molinari, A., Canova, G.-R., Ahzi, S., 1987. A self-consistent approach of the large deformation polycrystal viscoplasticity. Acta Metall. 35 (12), 2983–2994.

Mori, T., Tanaka, K., 1973. Average stress in a matrix and average elastic energy of materials with misfitting inclusions. Acta Metall. Mater. 42 (7), 597–629.

Pierard, O., Doghri, I., 2006. A study of various estimates of the macroscopic tangent operator in the incremental homogenization of elasto-plastic composites. Int. J. Mult. Comp. Eng. 4 (4), 521–543.

Ponte-Castañeda, P., Suquet, P., 1998. Nonlinear composites. Adv. Appl. Mech. 34, 171–302.
Ponte-Castañeda, P., Willis, J.-R., 1995. The effect of spatial distribution of effective behavior of composite materials and cracked media. J. Mech. Phys. Solids 43, 1919–1951.
Ponte-Castañeda, P., 1991. The effective mechanical properties of nonlinear isotropic composites. J. Mech. Phys. Solids 39, 45–71.
Shao, J.-F., Jia, Y., Kondo, D., Chiarelli, A.-S., 2006. A coupled elastoplastic damage model for semi-brittle materials and extension to unsaturated conditions. Mech. Mater. 38 (3), 218–232.
Shao, J.-F., Zhou, H., Chau, T., 2005. Coupling between anisotropic damage and permeability variation in brittle rocks. Int. J. Numer. Anal. Methods Geomech. 29 (12), 1231–1247.
Sibai, M., Dormieux, L., Pensée, V., Kondo, D., 2003. Effets de la microfissuration en poroélasticité des roches: étude expérimentale et analyse micromécanique. 16th French Mechanics Congres, Nice.
Tandon, G.-P., Weng, G.-J., 1988. A theory of particle-reinforced plasticity. J. Appl. Mech. Trans. ASME 55, 126–135.
Welemane, H., Cormery, F., 2003. An alternative 3d model for damage induced anisotropy and unilateral effect in microcracked materials. J. Phys. 105, 329–336.
Willis, J.-R., 1989. The structure of overall constitutive relations for a class of nonlinear composites. J. Appl. Math. 43, 231–242.